

Nonreciprocal ultrastrong magnon-photon coupling in the bandgap of photonic crystals

Chi Zhang,¹ Zhenhui Hao,¹ Yongzhang Shi,¹ Changjun Jiang,¹ C. K. Ong^{1,2}, and Guozhi Chai^{1*}

¹Key Laboratory for Magnetism and Magnetic Materials of the Ministry of Education, Lanzhou University, Lanzhou, 730000, People's Republic of China.

²Department of Physics, Xiamen University Malaysia, Jalan Sunsuria, Bandar Sunsuria, 43900, Sepang, Selangor, Malaysia.

(Dated: April 20, 2023)

We observe a nonreciprocal ultrastrong magnon-photon coupling in the bandgap of photonic crystals by introducing a single crystal YIG cylinder into copper photonic crystals cavity as a point defect. The coupling strength reaches up to 1.18 GHz, which constitutes about 10.9% of the photon energy compared to the photon frequency around 10.8 GHz. It is fascinating that the coupling achieves unidirectional signal transmission in the whole bandgap. This study demonstrates the possibility of controlling nonreciprocal magnon-photon coupling by manipulating the structure of photonic crystals, providing new methods to investigate the influence of magnetic point defects on microwave signal transmission.

I. INTRODUCTION

Cavity magnonics, which is based on coupling between magnons and cavity photons, has become a powerful platform for studying the hybrid quantum systems [1–5]. In this regime, information is carried and transmitted by the polarons that are generated by the coupling between magnons and photons. Since Soykal and Flatté proposed magnon-photon coupling (MPC) in 2010 [6, 7], many studies have demonstrated it in experiments and theories. Huebl et al. achieved a strong coupling with YIG films and coplanar waveguides at mK temperatures in 2013 [8]. Soon after, Zhang et al. accomplished experiments at room temperatures with an yttrium iron garnet (YIG) sphere and a three-dimensional (3D) microwave cavity [9]. A number of researchers have also reported a lot of interesting and valuable studies, like dissipative couplings [10, 11], indirect couplings [12–14], nonreciprocal couplings [15–18] in coupled systems. These studies show great promise in a wide range of applications in quantum information processing. Most importantly, strong coupling is necessary in the coupling system for broadening the frequency range. Researchers have achieved the strong MPC in different cavity systems with the magnons which have large spin density, such as 3D rectangular cavity [19, 20], split-ring resonator [21–23], inverted pattern of split-ring resonator [11], cross-line cavity [15] and photonic crystals (PCs) [24].

PCs are a kind of artificial inhomogeneous electromagnetic structures with definite refractive index or periodic dielectric constant [25–27]. Wang et al. introduced one-way modes analogous to quantum Hall edge states generalized with gyromagnetic materials [28], and observed the so-called chiral edge states [29] as well as in other research area [30–33]. In 2015, Skirlo et al. constructed a ferrimagnetic PCs with a band structure com-

prising high Chern numbers and the dispersion relations of one-way edge modes for the first time in any quantum Hall effect or quantum anomalous Hall effect system [34]. Liu and Houck discovered an attractive experimental phenomenon that a hybridization induced by the strong MPC can create localized cavity modes that live within the photonic bandgap [35]. Built on these interesting investigations, we realized an ultrastrong MPC with a coupling strength of 1.05 GHz and the coupling efficiency comes up to 11.7% in PCs with a ferrimagnetic point defect in 2019 [24]. This research indicates that PCs is an appropriate system to investigate the cavity magnonics.

In this work, a nonreciprocal ultrastrong coupling is realized in the band gap of the PCs with a magnetic point defect. Results show an ultrastrong interaction between the ferromagnetic resonance (FMR) mode and the defect mode of the PCs. In addition to broken time-reversal symmetry (TRS) of the system, microwave is allowed to transmit along one direction in the bandgap by tuning strength and direction of the applied magnetic field.

II. EXPERIMENTS

As illustrated in Fig. 1, our device consists of a 2D PCs with a point defect by substituting a YIG cylinder for a copper cylinder. A 2D chamber is constructed by two aluminum plates with 5mm of separation and surrounded by some microwave absorbing materials. All of the cylinders which have a diameter and a height as 5 mm are placed in the chamber and the lattice constant of the 2D simple cubic structure is defined as 20 mm. A vector network analyzer (VNA, Agilent E8363B) is employed to feed microwaves by connecting to two antennas. Meanwhile, a static magnetic field along z direction is applied by an electromagnet. We choose a single crystal YIG as the magnetic material because of its low microwave magnetic-loss parameter and high-spin-density [36]. Our YIG has a saturation magnetization $M_s = 1750$ G, a gy-

* Correspondence email address: chaigzh@lzu.edu.cn

romagnetic ratio $\gamma = 2.8$ MHz/Oe, and a linewidth of 10 Oe.

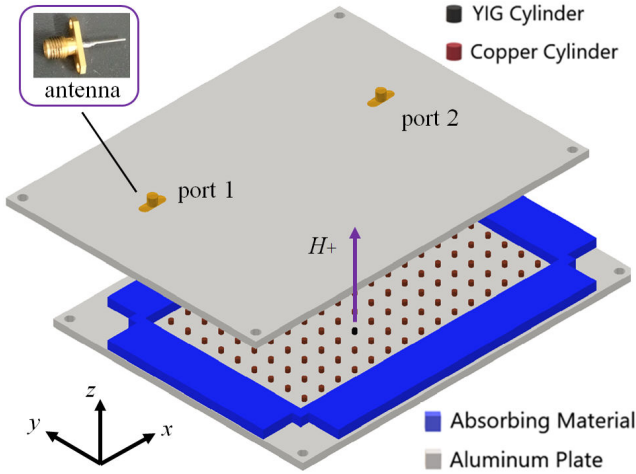


FIG. 1. Sketch of the experimental setup. The two-dimensional copper cylinder PCs with a point defect of a YIG cylinder. All cylinders have a diameter of 5 mm and a height of 5 mm. The lattice constant is 20 mm. Two aluminum plates are applied to be the two-dimensional chamber with 5 mm of separation and surrounded by some microwave absorbing materials. Microwave signals are supplied by a VNA through two microwave cables with two antennas. The static magnetic field is applied in the z direction.

The scatter parameter S_{ij} ($i, j = 1, 2$) is measured to characterize the experimental phenomena discussed subsequently. S_{ij} represents the microwave transmission signal from port j to port i . Figure 2(a) denotes the transmission coefficients S_{21} of copper cylinder PCs and YIG defect PCs as a function of frequency. Additional simulation results are introduced to understand experimental results. The microwave magnetic field distribution at 10.8 GHz in PCs and YIG defect PCs are illustrated as Figs. 2(b) and 2(c), respectively. It reveals that a strong gathering of the magnetic energy could be observed at the position of YIG cylinder [black circle on Fig. 2(c)]. It implies a localized mode within the band gap is excited. Focus on this eigen mode, we swept the applied static magnetic fields with a frequency range between 10.0 and 11.5 GHz.

III. RESULTS AND DISCUSSION

The density mapping image of the magnitude of transmission coefficient is shown in Fig. 3. Figures 3(a) and 3(b) display the density mapping images of the magnitude of the microwave transmission coefficient S_{21} and S_{12} , respectively. The spectra were measured by altering the static magnetic field H from -9000 to 9000 Oe with a step size of 18 Oe. An anti-crossing behavior arises owing to the coupling between magnons and photons. According to our experiments, magnons are supplied by

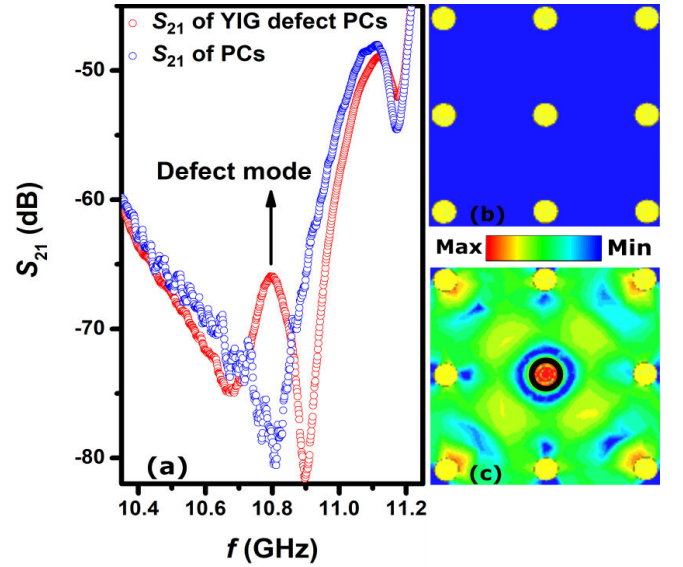


FIG. 2. (a) Experiment data. Microwave transmission coefficients S_{21} of the PCs and YIG defect PCs as a function of frequency. (b) and (c) represents the simulation of the microwave magnetic field distribution of the PCs and YIG defect PCs at 10.9 GHz, respectively. Black circle stands for the position of the YIG cylinder.

FMR mode and the photons are introduced by the eigen defect mode of the microwave cavity. The FMR mode (black dashed line in Fig. 3) is calculated by the Kittel equation [37]:

$$f_K = \gamma \sqrt{(H + (N_x - N_z)M_s)(H + (N_y - N_z)M_s)}. \quad (1)$$

The demagnetizing factors cannot be calculated analytically as the demagnetizing field is not uniform in cylindrical shape magnetized bodies. We choose the experiment results of the demagnetizing factors of the cylinder with the same dimensional ratio in the textbook [38]. Consequently, demagnetizing factors N_x , N_y and N_z are set a value as 0.365, 0.365 and 0.27, respectively. The frequency of photon defect mode f_{PC} is 10.8 GHz (red dashed line in Fig. 3). As shown in Fig. 3, the coupling displayed in the density mapping images of the transmission coefficients S_{ij} are reversed while the direction of applied magnetic field H is opposite. In addition, the S_{21} and S_{12} transmission coefficients are reversed also at the same direction of H . The results indicate a nonreciprocity with chirality in the system.

Unlike the nonreciprocal microwave transmission induced by the cooperative effect of coherent and dissipative coupling in an open cavity magnonic system [15], the nonreciprocity arises from the gyromagnetism of YIG cylinder and the spatial symmetry breaking of PCs with a defect in this work. The gyromagnetism of the YIG cylinder enhances in the vicinity of the resonance field, which reported in some previous studies [30–33]. Specifically, the permeability μ will turn into a second-rank

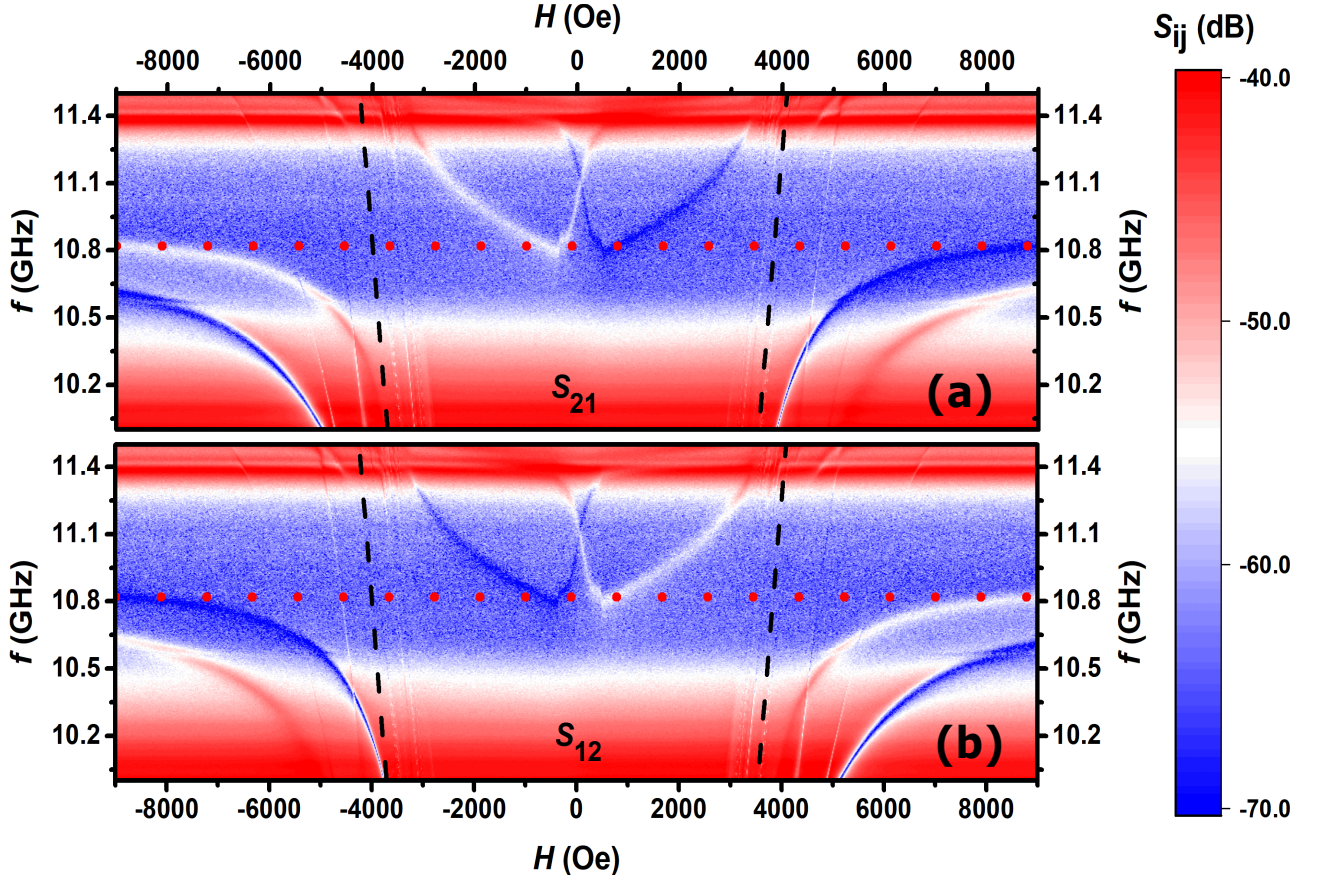


FIG. 3. The density mapping image of the amplitude of the transmission coefficients through the PCs cavity as a function of frequency f and the applied static magnetic field H . The closer the color to blue, the larger is the microwave transmission loss. (a) S_{21} mapping. (b) S_{12} mapping. Black dashed line indicates the FMR mode fitting with the Kittel equation [Eq. 1] and red dots represents the photon mode. S_{21} and S_{12} are reversed with the same direction of H in the region of coupled resonances. S_{21} or S_{12} is reversed with the opposite direction of H in the region of coupled resonances.

tensor $\boldsymbol{\mu}$ as the the microwave magnetic field is perpendicular to the applied magnetic field H . $\boldsymbol{\mu}$ is given by:

$$\boldsymbol{\mu} = \begin{pmatrix} \mu_r & -i\mu_i & 0 \\ i\mu_i & \mu_r & 0 \\ 0 & 0 & 1 \end{pmatrix}, \quad (2)$$

where $\mu_r = 1 + f_0 f_m / (f_0^2 - f^2)$, which represents the in-plane permeability, $\mu_i = -f f_m / (f_0^2 - f^2)$. Here, $f_m = \gamma M_s$ is the characteristic frequency [39]. The off-diagonal element in the permeability tensor is induced by the nonzero applied static magnetic field, which breaks the TRS directly [40]. The degree of breakage of TRS is characterized as $u = \mu_i / \mu_r$ [31]. For instance, u comes up to a value of 98.9% as $H = 2000$ Oe and $f = 11.0$ GHz. This implies a near complete TRS breaking.

Additionally, the magnetic defect is not located on the axis of symmetry of the PCs, spatial symmetry of the PCs cavity is broken, which is also helpful for breaking the TRS of the system (Researchers often introduce ferrites into resonant cavities with irregular shapes to break

the TRS of the systems in many studies about quantum chaos.) [41–44]. Above of all, the nonreciprocity can be attributed to the change in the rotational direction resulting from the interchange of the input and output channels, which based on the properties of special cavity magnonic system in this work.

We next calculate the coupling strength between YIG FMR mode and defect mode of YIG defect PCs. Firstly, the microwave photon and FMR are described by the Hamiltonian with a rotating-wave approximation (RWA) [9]:

$$\mathcal{H} = \begin{pmatrix} f_K + i\alpha & g \\ g & f_P + i\beta \end{pmatrix}. \quad (3)$$

The coupling curves are calculated by the two-mode model [8]:

$$f_{\pm} = \frac{1}{2}(f_P + f_K) \pm \frac{1}{2}\sqrt{(f_P - f_K)^2 + (2g/2\pi)^2}, \quad (4)$$

where f_P is the photon frequency of the defect mode, f_{\pm} are frequencies of the coupled resonances and $g/2\pi$

is the coupling strength with a value of 1.18 GHz. As shown in Fig. 4, f_{\pm} are described by green solid lines. The calculated coupling efficiency $g/(2\pi f_p) = 10.9\%$ of the photon energy when $f_p = 10.8$ GHz of the photon mode which is qualified as ultrastrong coupling [45]. In the ultrastrong coupling region, the stronger the coupling strength, the stronger is the nonreciprocity [17].

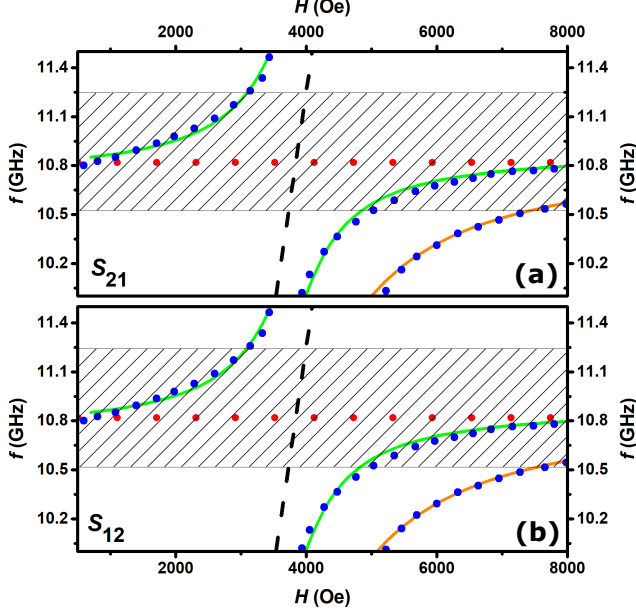


FIG. 4. The couplings in the frequency versus applied static magnetic field with the fitting curves. (a) S_{21} direction; (b) S_{12} direction. The experiment data are described as blue circles. Black dashed line indicates the FMR mode fitting with the Kittel equation [Eq. 1]; red dots indicate the photon frequency of defect mode located at 10.8 GHz; green curves are coupling curves fitting with the two-mode model [Eq. 4]. Bandgap is marked by dashed gray box.

Right bottom of Fig. 4 reveals another ultrastrong MPC expressed in orange curve. We design another experiment to understand the nature of the coupling. Note that the magnon mode and photon mode are provided by the YIG cylinder simultaneously [46–48].

As shown in the inset of Fig. 5(a), a microwave coaxial connector connected to the VNA is used to feed microwaves for the YIG cylinder. In this system, YIG cylinder is regarded as a microwave cavity itself and the first eigenmode is discovered at 12.2 GHz which is evident from Fig. 5(a). Correspondingly, this eigenmode could be regarded as the photon mode to interact with FMR mode. Subsequently, we applied static magnetic field H on the YIG to discover the variation of the microwave reflection coefficients S_{11} . As anticipated, we observed an anticrossing phenomenon caused by FMR mode and photon mode of the YIG. In Fig. 5(b) details of the spectrum of the coupling in the frequency versus applied static magnetic field, blue dots stand for the experiment data, black and red dashed lines represents FMR mode and photon mode of YIG cylinder, respectively. The cou-

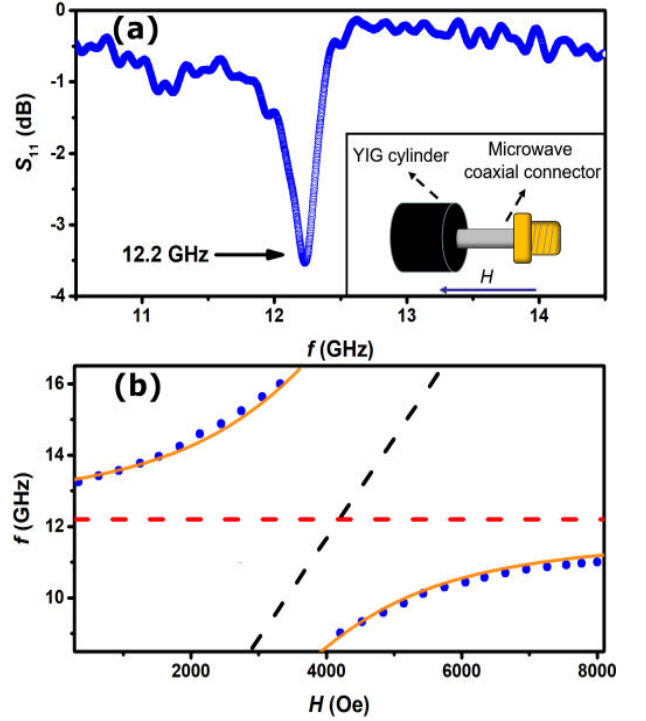


FIG. 5. (a) Microwave reflection coefficient S_{11} raw data of the YIG cylinder as a function of frequency at the magnetic field of 0. The inset stands for the experiment system. (b) The couplings in the frequency versus applied static magnetic field with the fitting curves. The experiment data are described as blue circles. Black dashed line indicates the FMR mode fitting with the Kittel equation [Eq. 1]; red dashed line indicates the resonance frequency of photon mode located at 12.2 GHz; orange curves are coupling curves fitting with the two-mode model [Eq. 5].

pling curves could be fit by two-mode model also:

$$f'_{\pm} = \frac{1}{2} (f_Y + f_K) \pm \frac{1}{2} \sqrt{(f_Y - f_K)^2 + (2g'/2\pi)^2}, \quad (5)$$

where f_Y is the photon frequency of the defect mode, f'_{\pm} are frequencies of the coupled resonances and $g'/2\pi$ is the coupling strength with a value of 4 GHz. As shown in Fig. 5, f'_{-} is described by orange curve. It is observed from the results that polarization mode f'_{-} is adaptive for orange solid line as shown in Fig. 4.

IV. SUMMARY

In summary, we introduces a magnetic point defect by replacing a copper cylinder with a single crystal YIG cylinder, which is not located on the axis of symmetry in the 2D simple cubic metal PCs, breaking the spatial symmetry of the system. A defect mode at a frequency of 10.8 GHz in the bandgap could be found. This defect mode can be regarded as a photon mode that couples with the FMR mode of YIG, with a coupling strength

of 1.18 GHz. As the coupling efficiency exceeding 10%, reaching up to 10.9%, the coupling can be considered as an ultrastrong MPC. Furthermore, the coupling displays strong nonreciprocity, enabling unidirectional microwave transmission within the bandgap of PCs. This study contributes to a better understanding of the magnetic defect in PCs, which is of great significance for exploring the fundamental principles and applications of PCs and for developing new microwave devices. In particular, it sheds some light on providing new ideas and directions for de-

vices used in the field of microwave filtering.

V. ACKNOWLEDGEMENTS

This work is supported by the National Natural Science Foundation of China (NSFC) (No. 12174165) and Natural Science Foundation of GanSu Province for Distinguished Young Scholars (No. 20JR10RA649).

-
- [1] X. Zhang, C.-L. Zou, L. Jiang, and H. X. Tang, *Sci. Adv.* **2**, e1501286 (2016).
- [2] M. Harder and C.-M. Hu, *Solid State Phys.* **69**, 47 (2018).
- [3] B. Bhoi and S.-K. Kim, *Solid State Phys.* **70**, 1 (2019).
- [4] C.-M. Hu, *Solid State Phys.* **71**, 117 (2020).
- [5] B. Zare Rameshti, S. Viola Kusminskiy, J. A. Haigh, K. Usami, D. Lachance-Quirion, Y. Nakamura, C.-M. Hu, H. X. Tang, G. E. Bauer, and Y. M. Blanter, *Phys. Rep.* **979**, 1 (2022).
- [6] Ö. O. Soykal and M. E. Flatté, *Phys. Rev. Lett.* **104**, 077202 (2010).
- [7] Ö. O. Soykal and M. E. Flatté, *Phys. Rev. B* **82**, 104413 (2010).
- [8] H. Huebl, C. W. Zollitsch, J. Lotze, F. Hocke, M. Greifenstein, A. Marx, R. Gross, and S. T. B. Goennenwein, *Phys. Rev. Lett.* **111**, 127003 (2013).
- [9] X. Zhang, C.-L. Zou, L. Jiang, and H. X. Tang, *Phys. Rev. Lett.* **113**, 156401 (2014).
- [10] M. Harder, Y. Yang, B. M. Yao, C. H. Yu, J. W. Rao, Y. S. Gui, R. L. Stamps, and C.-M. Hu, *Phys. Rev. Lett.* **121**, 137203 (2018).
- [11] B. Bhoi, B. Kim, S.-H. Jang, J. Kim, J. Yang, Y.-J. Cho, and S.-K. Kim, *Phys. Rev. B* **99**, 134426 (2019).
- [12] P. Hyde, L. Bai, M. Harder, C. Match, and C. M. Hu, *Appl. Phys. Lett.* **109**, 152405 (2016).
- [13] L. Bai, M. Harder, P. Hyde, Z. Zhang, C.-M. Hu, Y. P. Chen, and J. Q. Xiao, *Phys. Rev. Lett.* **118**, 217201 (2017).
- [14] J. Li, S.-Y. Zhu, and G. S. Agarwal, *Phys. Rev. Lett.* **121**, 203601 (2018).
- [15] Y.-P. Wang, J. W. Rao, Y. Yang, P.-C. Xu, Y. S. Gui, B. M. Yao, J. Q. You, and C.-M. Hu, *Phys. Rev. Lett.* **123**, 127202 (2019).
- [16] X. Zhang, K. Ding, X. Zhou, J. Xu, and D. Jin, *Phys. Rev. Lett.* **123**, 237202 (2019).
- [17] C. Zhang, C. Jia, Y. Shi, C. Jiang, D. Xue, C. K. Ong, and G. Chai, *Phys. Rev. B* **103**, 184427 (2021).
- [18] Y. Shi, C. Zhang, C. Jiang, C. K. Ong, and G. Chai, *Appl. Phys. Lett.* **119**, 132403 (2021).
- [19] Y.-P. Wang, G.-Q. Zhang, D. Zhang, T.-F. Li, C.-M. Hu, and J. Q. You, *Phys. Rev. Lett.* **120**, 057202 (2018).
- [20] L. Bai, M. Harder, Y. P. Chen, X. Fan, J. Q. Xiao, and C.-M. Hu, *Phys. Rev. Lett.* **114**, 227201 (2015).
- [21] B. Bhoi, T. Cliff, I. S. Maksymov, M. Kostylev, R. Aiyar, N. Venkataramani, S. Prasad, and R. L. Stamps, *J. Appl. Phys.* **116**, 243906 (2014).
- [22] D. Zhang, W. Song, and G. Chai, *J. Phys. D* **50**, 205003 (2017).
- [23] Y. Shi, D. Zhang, C. Zhang, C. Jiang, and G. Chai, *J. Phys. D* **52**, 305003 (2019).
- [24] C. Zhang, Y. Shi, W. Zhang, C. Jiang, and G. Chai, *Appl. Phys. Lett.* **115**, 022407 (2019).
- [25] E. Yablonovitch, *Phys. Rev. Lett.* **58**, 2059 (1987).
- [26] S. John, *Phys. Rev. Lett.* **58**, 2486 (1987).
- [27] J. D. Joannopoulos, S. G. Johnson, J. N. Winn, and R. D. Meade, *Photonic Crystals Molding the Flow of Light* (Princeton University Press, Princeton, 2008).
- [28] Z. Wang, Y. D. Chong, J. D. Joannopoulos, and M. Soljačić, *Phys. Rev. Lett.* **100**, 013905 (2008).
- [29] Z. Wang, Y. Chong, J. D. Joannopoulos, and M. Soljačić, *Nature* **461**, 772 (2009).
- [30] S. Liu, W. Chen, J. Du, Z. Lin, S. T. Chui, and C. T. Chan, *Phys. Rev. Lett.* **101**, 157407 (2008).
- [31] Y. Poo, R.-x. Wu, Z. Lin, Y. Yang, and C. T. Chan, *Phys. Rev. Lett.* **106**, 093903 (2011).
- [32] J. Lian, J.-X. Fu, L. Gan, and Z.-Y. Li, *Phys. Rev. B* **85**, 125108 (2012).
- [33] Y. Poo, R.-x. Wu, S. Liu, Y. Yang, Z. Lin, and S. T. Chui, *Appl. Phys. Lett.* **101**, 081912 (2012).
- [34] S. A. Skirlo, L. Lu, Y. Igarashi, Q. Yan, J. Joannopoulos, and M. Soljačić, *Phys. Rev. Lett.* **115**, 253901 (2015).
- [35] Y. Liu and A. A. Houck, *Nat. Phys.* **13**, 48 (2017).
- [36] A. A. Serga, A. V. Chumak, and B. Hillebrands, *J. Phys. D* **43**, 264002 (2010).
- [37] C. Kittel, *Phys. Rev.* **73**, 155 (1948).
- [38] S. Chikazumi, *Physics of Ferromagnetism* (Oxford University, New York, 1997).
- [39] J.-X. Fu, R.-J. Liu, and Z.-Y. Li, *Appl. Phys. Lett.* **97**, 041112 (2010).
- [40] P. So, S. M. Anlage, E. Ott, and R. N. Oerter, *Phys. Rev. Lett.* **74**, 2662 (1995).
- [41] B. Dietz, T. Friedrich, H. L. Harney, M. Miski-Oglu, A. Richter, F. Schäfer, J. Verbaarschot, and H. A. Weidenmüller, *Physical Review Letters* **103**, 064101 (2009).
- [42] B. Dietz, T. Guhr, H. L. Harney, and A. Richter, *Physical Review Letters* **96**, 254101 (2006).
- [43] B. Dietz, T. Klaus, M. Miski-Oglu, A. Richter, and M. Wunderle, *Physical Review Letters* **123**, 174101 (2019).
- [44] B. Dietz, T. Klaus, M. Miski-Oglu, A. Richter, M. Bischoff, L. von Smekal, and J. Wambach, *Physical Review Letters* **115**, 026801 (2015).
- [45] T. Niemczyk, F. Deppe, H. Huebl, E. Menzel, F. Hocke, M. Schwarz, J. Garcia-Ripoll, D. Zueco, T. Hümmer, E. Solano, *et al.*, *Nat. Phys.* **6**, 772 (2010).
- [46] B. Zare Rameshti, Y. Cao, and G. E. W. Bauer, *Phys. Rev. B* **91**, 214430 (2015).

- [47] J. Bourhill, N. Kostylev, M. Goryachev, D. L. Creedon, and M. E. Tobar, *Phys. Rev. B* **93**, 144420 (2016).
- [48] J. Krupka, A. Pacewicz, B. Salski, P. Kopyt, J. Bourhill, M. Goryachev, and M. Tobar, *J. Magn. Magn. Mater.* **521**, 167536 (2021).